ChemPubSoc Europe

DOI: 10.1002/chem.201303489

CHEMISTRY
A European Journal
Full Paper

Single-Molecule Magnets | *Very Important Paper*

VIP Can Anisotropic Exchange Be Reliably Calculated Using Density Functional Methods? A Case Study on Trinuclear Mn^{III}-M^{III}-Mn^{III} (M = Fe, Ru, and Os) Cyanometalate Single-Molecule Magnets

Saurabh Kumar Singh and Gopalan Rajaraman*[a]

Abstract: Density functional studies have been performed on a set of trinuclear single-molecule magnets (SMMs) of general formula $[\{Mn_2(5\text{-Br salen})_2(MeOH)_2\}M(CN)_6](NEt_4)$ (M = Fe^{III} (**1**), Ru^{III} (**2**) and Os^{III} (**3**); 5-Brsalen = *N*,*N*′-ethylenebis(5-bromosalicylidene)iminato anion). We have computed the orbital-dependent exchange interaction for all three complexes for the first time using DFT and complete active space self-consistent field (CASSCF) methods. DFT calculations yield the anisotropic exchange as $J_{\xi\xi} = 3.5\ cm^{-1}$ for **1**; $J_{\xi\xi} = 12.1\ cm^{-1}$, $J_{\zeta\zeta} = -6.9\ cm^{-1}$ and $J_{\eta\eta} = -14\ cm^{-1}$ for **2**; and $J_{\xi\xi} = 23.7\ cm^{-1}$ and $J_{\zeta\zeta} = -11.1\ cm^{-1}$ for **3**. The computed values are in agreement with the experimental report, and this suggests that the established methodology can be used to compute the anisotropic exchange in larger clusters. Our calculations reiterate the fact that the exchange is described by a three-axis anisotropic exchange for complexes **2** and **3** as evidenced by the experiments. A stronger exchange coupling as we move down the periodic table from 3d to 5d is reproduced by our calculations, and the origin of this enhancement in the exchange interaction has been probed by using molecular orbital analysis. The electronic origin of different types of exchange observed in this series is found to be related to the energy difference between possible degenerate pairs and the nature of orbital interactions. By computing the exchange interaction, the single-ion anisotropy of Mn^{III} and zero-field splitting of the $S = {}^9/_2$ ground state of complexes **1**–**3** using CASSCF and/or DFT methods, we have attempted to shed light on the issue of anisotropic exchange and the barrier height for the magnetisation reversal in SMMs. Comprehensive magneto–structural correlations have been developed to offer clues on how to further enhance the barrier height in this class of SMMs.

Introduction

Single-molecule magnets (SMMs)[1] have gained attention in recent years as numerous potential applications are proposed for this class of molecules. Such application range from high-density information storage devices to solid-state Q-bits in quantum computing.[1,2] Enhancing the barrier height (related to the spin ground-state *S* and axial zero-field splitting *D*) for the reorientation of magnetisation in SMMs remains one of the primary challenges in bringing these molecules to end-user applications. Over the last decade, hundreds of SMMs that contain transition-metal ions have been reported,[4] and a notable achievement in this regard is the report by Brechin et al.[5] on the synthesis of an $\{Mn_6^{III}\}$ SMM with a record barrier height of 86 K.

There are essentially two approaches for the synthesis of large clusters. The first approach concerns self-assembly[6] in which metal ions are aggregated using oxygen/nitrogen or other donor ligands. Numerous clusters have been synthesised using this methodology including the archetypal $\{Mn_{12}\}$ cluster[7] and clusters as large as $\{Mn_{84}\}$.[8] The second is a rational approach in which targeted clusters are synthesised generally by using ligands that yield predictable structures such as cyanides[9a] or rigid ligands such as β-diketone[10] and many others.[11,12] Although this methodology yields comparatively smaller-nuclearity clusters, it offers a way to design the structure/properties beforehand. This methodology also enjoys the advantage of controlling the symmetry of the structure as illustrated by several highly symmetric[13] cyanometalate clusters. In addition, because cyanides are a strong-field ligand they preserve the orbital degeneracy of the coordinated metal ions in many cases,[14] which leads to a large anisotropy,[9,11,12] one of the primary but difficult to achieve requirements for SMMs.

In recent decades much attention has been paid to the synthesis of Prussian blue analogues.[15] One of the challenges often encountered with this class of molecules is the nature of the exchange interaction, which is generally weak, and the estimated anisotropy, which is rather moderate.[16,17] To overcome this challenge, mixed 3d–4d and 3d–5d cyanometalate clusters have been synthesised.[16] The larger diffused d orbitals for 4d and 5d ions relative to the 3d series offer a unique way to enhance the strength of the exchange interaction. Furthermore, these ions also inherit a large anisotropy on account of their larger spin–orbit coupling than 3d metal ions, and thus offer large magnetic anisotropy to the cluster compound. The ad-

[a] *S. K. Singh, Prof. G. Rajaraman*
Department of Chemistry, Indian Institute of Technology Bombay
Powai, Mumbai-400076 (India)
Fax: +91-(0)22-2576-7152
E-mail: rajaraman@chem.iitb.ac.in

Supporting information for this article is available on the WWW under http://dx.doi.org/10.1002/chem.201303489.

vantage of using 4d and 5d metal ions in building SMMs has recently been highlighted by Dunbar et al.[17] Furthermore, the 4d and 5d metal ions also exhibit anisotropic exchange, which is a promising parameter to build higher-blocking-temperature SMMs.[18] This class of molecules is also important from the perspective of photomagnetism,[19] spin-crossover complexes[20] and single-chain magnets.[21]

One of the challenges yet to be fully addressed in this area is a perceivable way to control the pairwise interaction between the metal ions. The sign as well the strength of the exchange interaction (*J*) is vital for the development of futuristic magnetic materials.[6] Enhancing the magnitude of the exchange interaction for a given molecule is a non-trivial task. By using more-diffuse late-transition metals, Girolami and Entley[22] initially demonstrated that the magnitude of the *J* value can be significantly enhanced. Owing to a large electron density on the π^* orbital of cyanide ions, these cyanometalates also offer relatively larger *J* values than ligands such as carboxylates or phosphonates, which are also used frequently in cluster aggregation.[23,24]

The synthesis of novel {3d–4d/5d} SMMs demands a thorough understanding and a perceivable way to achieve control of microscopic spin-Hamiltonian parameters. Theoretical tools are invaluable in this area as these molecules can be too complex to address experimentally and numerous predictions have been made using theoretical methods.[25] Some milestone achievements among others[11,18,25] in this area include 1) Ruiz et al., using the pairwise model, estimated the magnetic exchange in several cyanometalate complexes and have demonstrated the robustness of DFT in estimating the *J* values in this class of compounds;[26] 2) a methodology proposed by Atanasov et al. to calculate the *J* values using computed spin densities and ligand-field-aided DFT methods[11] and the role of Jahn–Teller (J–T) distortion in the magnetic anisotropy of SMMs; and 3) Mironov et al, who proposed a methodology to extract anisotropic exchange in cyanide-based clusters using kinetic exchange theory and offered insight into the nature of anisotropic exchange in SMMs.[18,27]

One of the seminal works reported in this area is due to Pederson et al.,[28–30] who synthesised a series of trinuclear SMMs with the molecular formula of $[(NEt_4)\{Mn_2(5\text{-Brsalen})_2(MeOH)_2\}M(CN)_6]$ ($M = Fe^{III}$, Ru^{III} and Os^{III}; 5-Brsalen = *N*,*N*′-ethylenebis(5-bromosalicylidene)iminato anion). All three compounds are characterised as SMMs with a barrier height of 17 and 19 K for Ru and Os complexes, respectively, and much lower barrier height for the Fe analogue.[28] There are also a few other reports of trinuclear Mn^{III}-based cyanometalates that possess SMM characteristics. Long et al. synthesised an {Mn-Fe-Mn} complex[31] with an effective barrier height (U_{eff}) of 35.7 K. Ferbinteanu et al. have reported a similar {Mn-Fe-Mn} trinuclear complex with Me–Salen (Salen = *N*,*N*′-ethylenebis(salicylimine)) ligand with an estimated U_{eff} of 14 K.[32] Piggott et al. have reported several 3d metal-ion analogues like {Mn-Co-Mn}, {Mn-Cr-Mn} and {Mn-Fe-Mn}, which possess SMM characteristics.[32,34] Although several Mn^{III}–Fe^{III} cyanometalate SMMs have been reported, in none of the cases were their 4d/5d congeners found to be SMMs except in the work of Pederson et al.[28,29] Their report of 3d–4d/5d SMMs is the first of its kind, and because these SMMs were found to be better than the 3d–3d analogues, this made us more curious to determine the role of 4d and 5d ions in magnetic coupling as well as anisotropy.

To understand the nature of interaction and the origin of the magnetic anisotropy, we have chosen the series of trinuclear complexes $[(NEt_4)\{Mn_2(5\text{-Brsalen})_2(MeOH)_2\}M(CN)_6]$ (in which $M = Fe^{III}$ (**1**), Ru^{III} (**2**) and Os^{III} (**3**)) reported by Pederson et al.[28–30] and subjected it to comprehensive electronic structure studies using density functional methods. Herein, apart from estimating the isotropic exchange, we have also computed the orbital-dependent exchange by using DFT methods for selected cases. In addition, the ab initio and DFT approaches have been utilised to estimate the zero-field splitting (*D* tensor) for all three complexes. In general, all our computed parameters are in good agreement with the experiments. Moreover, we have performed MO analysis to understand the mechanism of magnetic coupling in this 3d–4d/3d–5d class of compounds. We have also developed several magneto–structural correlations to figure out the most influential structural parameter that is strongly correlated to the magnitude as well the sign of the exchange interaction.

Computational Methods

In these trinuclear complexes, the magnetic exchange interactions between Mn^{III} and M^{III} (Fe, Ru and Os) and Mn^{III}–Mn^{III} 1,3 interactions were computed using the pairwise interaction model,[35] in which four spin configurations were computed to extract three different exchange interactions (J_1–J_3; see below). The following four configurations have been computed: 1) all spin up ($S = {}^9/_2$), 2) spin down on Mn_A ($S = {}^1/_2$), 3) spin down on Mn_B ($S = {}^1/_2$) and 4) spin down on M^{III} (M = Os, Fe) ($S = {}^7/_2$). The energy difference between spin configurations is equated to the corresponding pairwise exchange interaction from which all three *J* values have been extracted.

The following spin Hamiltonian is used to describe the isotropic magnetic exchange interaction in complexes **1**–**3** [Eq. (1)]:

$$\hat{H} = -J_1 S_{Mn_1} S_{Os} - J_2 S_{Os} S_{Mn_2} - J_3 S_{Mn_1} S_{Mn_2} \quad (1)$$

DFT combined with the broken-symmetry (BS) approach has been employed to compute the energies of the different spin configurations. The BS method has proven the track record of yielding a good numerical estimate of *J* values for a variety of complexes.[13,10] Here we have performed most of our calculations using the Gaussian 09 suite of programs.[36] We have employed a hybrid B3LYP functional[37] along with relativistic effective-core potential LANL08f on Os, Ru and Fe atoms.[38] The Br atom was treated with the LANL2DZ effective-core potential basis set[39] and the rest of the elements were treated with Ahlrichs triple-ζ TZV basis set.[40] The self-consistent field (SCF) convergence to the desired solution is challenging for trinuclear complexes and here we have employed multiple ways to tackle the issue: among others the fragment approach, which offers a way to control the local spin on the metal ions as implemented in Gaussian 09, has been used. The higher-energy configurations were then obtained by visualising the orbitals and performing orbital rotations by using variable shift, which eventually reaches the default Gaussian 09 values.

The ZFS calculations were performed using the ORCA suite of programmes.[41] We have performed DFT as well as ab initio complete active space self-consistent field (CASSCF) theory/N-electron valence perturbation theory (NEVPT2) calculations for the estimation of *D* and *g* tensors for complexes **1**–**3**. The DFT calculations for *D* tensors were carried out with quasi-degenerate theory[42] and the spin–orbit mean field approach (SOMF). The Ahlrichs TZVPPP basis set was used for Mn^{III};[40] a triple-ζ valence basis set for 3d/4d/5d metal ions;[40,43] and a triple-ζ valence basis set for Br were employed during the calculations, and the rest of the atoms were treated with the Ahlrichs TZV basis set.[40] The *D*-tensor calculations have been performed by incorporating the relativistic effect by means of the zeroth-order regular approximation (ZORA) as implemented in ORCA. We used the coupled perturbed (CP) spin–orbit coupling (SOC) approach to evaluate D_{SOC}, and the spin–spin contribution (D_{SS}) is estimated through the unrestricted natural orbital (UNO) method implemented in ORCA. Previous studies suggest that the DFT studies with the UNO approach for D_{SS} and the CP approach for D_{SOC} are the best combinations to obtain accurate zero-field splitting (ZFS) parameters.[44] The *D*-tensor calculations were also performed by incorporating relativistic effects by means of the Doughlas–Kroll–Hess method.[45] In the ab initio framework, all the calculations have been based on the CASSCF methodology, and we have also focused our attention on the importance on low-lying excited states. The spin–orbit coupling plays an important role in the estimation of the ZFS parameter. Four active electrons occupying the five metal d-based orbitals of Mn^{III} has been taken as the reference space for our CASSCF calculations. In our system we have considered the following low-lying excited states: 1) five quintet and 2) 35 triplet excited states for the estimation of the single-ion anisotropy of the Mn^{III} ions.[44] The calculations were performed with the TZVPPP basis set for all atoms on a model complex of **3**. To investigate the impact of dynamic correlation on the predictions, we have used the recently implemented NEVPT2 method.[46] A tight convergence has been employed throughout.

Furthermore, we have computed the Kramers doublets that arise from the $^2T_{2g}$ configuration for Os^{III}/Ru^{III}/Fe^{III} analogues to determine the energies of the different Kramers doublets and to understand their role in manifesting the magnetic anisotropy in these complexes. All these calculations were carried out on the model complexes using the RASSI-SO module in MOLCAS 7.6.[47]

Results and Discussion

All three structures **1**–**3** were found to be isostructural (see Figure 1), with the trinuclear molecules possessing two Mn^{III} atoms capped by the substituted Salen ligand and the hexacyano Fe^{III}/Ru^{III}/Os^{III} at the centre in *trans*-coordination mode, thus yielding near-linear structures. The Mn^{III} atoms exhibit J–T distortion, and the elongated axes are found to be along the bridging direction. Selected structural parameters for complexes **1**–**3** are given in Table 1.

Exchange interaction in trinuclear {Mn^{III}-M^{III}-Mn^{III}} complexes

Our initial focus was to compute the magnetic exchange interactions in all three complexes. Much of our attention was paid to the Os^{III} analogue as this is the best SMM among the reported series, and computations have been extended to Fe^{III} and Ru^{III} complexes for comparison. The $[Os(CN)_6]^{3-}$ under a strong octahedral ligand-field environment has a low-spin d^5 configuration to yield a $^2T_{2g}$ ground state. The strength of the spin–orbit coupling and the distortion from the ideal octahedral environment in the above complex essentially lead to splitting of the ground state. The degeneracy within the t_{2g}-like orbitals (d_{xy}, d_{yz} and d_{xz}) essentially leads to orbital-dependent (anisotropic) exchange. Our DFT calculations on **3** performed on high-spin state ($S = {}^9/_2$) yield the following as the ground-state configuration for Os^{III}: $(d_{xz})^2(d_{yz})^2(d_{xy})^1$ with the unpaired electron residing on the δ-type d_{xy} orbital. To check whether we have obtained a correct ground state for the Os^{III}, Ru^{III} and Fe^{III} configurations and to unequivocally evaluate the correct ground-state configurations, we performed ab initio CASSCF calculations with the reference space consisting of all d-based orbitals of Os^{III} on a monomeric model system and have computed three low-lying roots with the reference space of (5,5). The calculations confirm that the solution with the unpaired electron residing in the d_{xy} δ-type orbital is the ground state, with the other two roots found to be 0.04 and 0.1 eV higher in energy (see Figure 2). Within the ground state, the d_{xy} orbital was found to have the weight-age of 90% relative to the d_{xz} and d_{yz} orbitals, and this validates the accuracy of a single-determinant solution such as B3LYP for the studied examples. Furthermore, we have also performed an SA-CASSCF calculation on the trinuclear complex that incorporates the Mn^{III} and

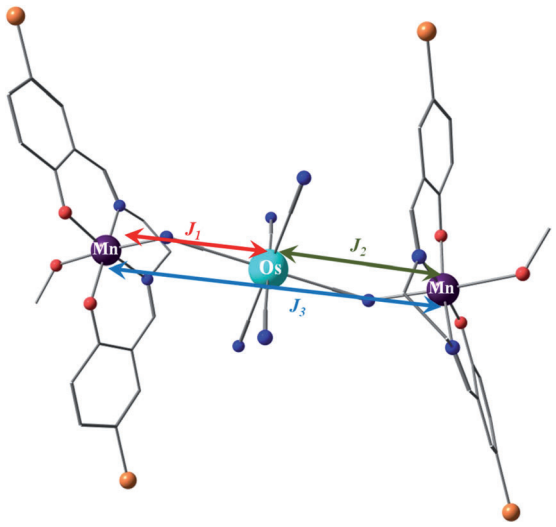

Figure 1. Crystal structure of [Mn^{III}-Os^{III}-Mn^{III}] trinuclear complex. Colour scheme is cyan: Os^{III}, violet: Mn^{III}, light brown: Br, blue: N, grey: C. Hydrogen atoms are omitted for clarity. The exchanges J_1–J_3 are shown with double-headed arrows. See text for details.

Table 1. Selected X-ray structural parameters of complexes **1**–**3**.

Complexes	Mn-Fe-Mn	Mn-Ru-Mn	Mn-Os-Mn
Mn–N [Å]	2.253	2.250	2.252
Fe/Ru/Os-C-N [°]	176.6	175.9	176.2
Mn-N-C [°]	145.3	144.1	143.3
Mn–M_A [Å]	5.081	5.163	5.167
Mn–M_B [Å]	5.081	5.163	5.167
C-M-N-Mn [°]	13.5	14.0	14.1
M–C [Å]	1.933	2.045	2.048

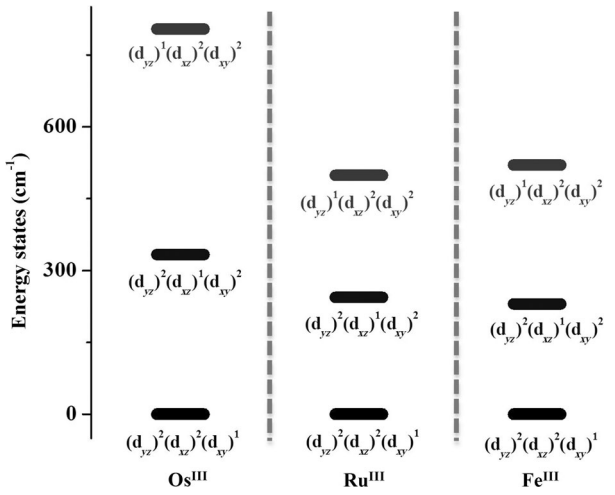

Figure 2. CASSCF-computed energy plot for three lowest-lying states for complexes **1**–**3** with their electronic configurations.

Os^{III} d-based orbitals in the reference space of (13,13) (only the e_g orbital of Os^{III} was neglected; see Table S1 in the Supporting Information for details), and this expansive calculation also suggested that the $(d_{xz})^2(d_{yz})^2(d_{xy})^1$ configuration for Os^{III} has more than 90% weight-age relative to other two configurations (see Table S1 in the Supporting Information). The predicted orbital ordering is also consistent with the ligand-field paradigm proposed earlier for the low-spin d^5 octahedral environment.[48] To explicitly include the spin–orbit coupling, we also performed RASSI-SO calculations on top of the converged CAS orbitals to compute the low-lying Kramers doublet. This procedure has routinely been used by Chibotaru et al. for heavier-transition-metal and lanthanide complexes.[49,50] The energies of the computed Kramers doublet are given in Table S2 of the Supporting Information, and this explicit incorporation of the SO effect also suggests significant mixing of the configurations discussed. Similar studies have also been undertaken for complexes **1** and **2** (see the Supporting Information for details)

The following exchange Hamiltonian generalises the orbital-dependent exchange that is applicable for the present scenario [Eq. (2)]:

$$\hat{H}_{\text{exe}}(\text{Mn}-\text{M}-\text{Mn}) = \sum_{\mu=\xi,\eta,\zeta} -J_{1\mu\mu}\hat{S}_1\hat{S}_{2\mu\mu} - J_{2\mu\mu}\hat{S}_{2\mu\mu}\hat{S}_3 - J_{3\mu\mu}\hat{S}_1\hat{S}_3 \quad (2)$$

in which $J_{1\text{–}3\mu\mu}$ ($\mu = \xi, \eta, \zeta$) are the exchange coupling constants between the unpaired spins of the Mn^{III} (S_1/S_3) and the spins $S_{2\mu}$ of the magnetic orbitals d_{xy} (ξ), d_{xz} (ζ), and d_{yz} (η) of M^{III} The M^{III}-C-N-Mn^{III} direction is taken as the *z* direction as this is found to be the J–T elongated axis as per the crystal structure parameters.

For complex **3** (see Table S3 in the Supporting Information), the DFT calculations yield $J_{1\xi\xi} = +23.7\ \text{cm}^{-1}$ and $J_{2\xi\xi} = +23.7\ \text{cm}^{-1}$ compared to the experimental value of $+25.5\ \text{cm}^{-1}$ in which $J_1 = J_2$ is assumed in the initial report.[28] A very similar Mn^{III} environment on both sides of Os^{III} yields a $J_1 \approx J_2$ scenario, and this is consistent with the experimental approximation. The 1,3 Mn–Mn J_3 interaction is computed to be very small ($+0.01\ \text{cm}^{-1}$), which stands in contrast to relatively larger values proposed by experiments ($+3.2\ \text{cm}^{-1}$) (see the computed energies and the expectation values in Table S3 of the Supporting Information and Figure 1 for a pictorial representation of *J* values). To estimate the orbital-dependent exchange, we have swapped the unpaired electron from the ground-state δ-type d_{xy} orbital to the π-type d_{xz} (M^{III} $(d_{xy})^2(d_{yz})^2(d_{xz})^1$) and then to the π-type d_{yz} (M^{III} $(d_{xy})^2(d_{xz})^2(d_{yz})^1$) orbital within the DFT framework and estimated the exchange interaction for each of the configurations. For complex **3** the $J_{1\zeta\zeta}$ value is estimated to be $-11.1\ \text{cm}^{-1}$. Due to the difficulty with convergence of one solution, we were unable to estimate the $J_{1\eta\eta}$ for complex **3**. The full set of DFT-calculated values for complex **2** is given in Table 2 (see all DFT-computed energies in Table S5 of the Supporting Information). Recently, Dreiser et al.[30] employed direct current (dc) magnetic susceptibility and frequency-domain Fourier-transform THz-EPR (FDFT THz-EPR) to study the magnetic properties of complex **3** and **2** and suggested that the magnetic exchange across the Mn–Os/Ru is highly anisotropic in nature with the estimate of $J_{1\xi\xi} = 35\ \text{cm}^{-1}$, $J_{1\zeta\zeta} = -18\ \text{cm}^{-1}$ and $J_{1\eta\eta} = -33\ \text{cm}^{-1}$ for **3** and $J_{1\xi\xi} = 25\ \text{cm}^{-1}$, $J_{1\zeta\zeta} = -20\ \text{cm}^{-1}$ and $J_{1\eta\eta} = -26\ \text{cm}^{-1}$ for complex **2**.[30] Although absolute values are slightly underestimated in DFT calculations, overall there is a good agreement in reproducing the sign as well the trend among the computed three-axis *J* values (see Tables 2 and 3). Compared to this new set of data, it is clear that our computed values reiterate the fact that the three-axis anisotropy is operational in these two complexes and this is consistent with experimental observations.[30] Moreover, the computed *J* values also provide a good fit to the magnetic susceptibility for complex **2** (see Figure S2 in the Supporting Information)

Table 2. Orbital-dependent exchange interaction: $J_{1\xi\xi}$, $J_{1\zeta\zeta}$ and $J_{1\eta\eta}$ for complex **2**.

Solutions	$J_{1\ \text{DFT}}$ [cm^{-1}]	$J_{1}'_{\text{DFT}}$ [cm^{-1}] (projected)	$J_{1}'_{\text{exp}}$ [cm^{-1}]
$\xi\xi$ $\{(d_{xz})^2(d_{yz})^2(d_{xy})^1\}$	12.1	7.5	7.5
$\zeta\zeta$ $\{(d_{xy})^2(d_{xz})^2(d_{xz})^1\}$	−6.9	−10	−9
$\eta\eta$ $\{(d_{xy})^2(d_{yz})^2(d_{yz})^1\}$	−14.1	−39	−76.5

In the absence of explicitly including the spin–orbit coupling, the Hamiltonian is described as shown in Equation (3):

$$\begin{pmatrix} J_{1\zeta\zeta} & 0 & 0 \\ 0 & J_{1\xi\xi} & 0 \\ 0 & 0 & J_{1\eta\eta} \end{pmatrix} \quad (3)$$

Inclusion of the spin–orbit coupling splits the $^2T_{2g}$ state and yields a Γ_7 doublet as the ground state. The effective Hamiltonian $\hat{H}_{\text{eff}}$ describes the exchange interaction between the Γ_7 doublet as the ground state and the projected spin of the Mn^{III} ions (see the Supporting Information for details). The effective spin Hamiltonian $\hat{H}_{\text{eff}}$ can be obtained by first-order perturba-

Table 3. DFT-computed magnetic exchange for complex **1**–**3** and experimental values.[a]

Complex		J_{DFT} [cm^{-1}]			J_{exp} [cm^{-1}]		
		J_1	J_2	J_3	J_1	J_2	J_3
{MnFeMn} **1**	$\xi\xi$	3.5	3.5	0.1	5.8	5.8	–
{MnRuMn} **2**	$\xi\xi$	12.1	12.1	0.09[a]	7.5	7.5	–
		(7.5)	*(7.5)*				–
	$\zeta\zeta$	−6.9	−6.9	0.06	−9.0	−9.0	–
		(−10)	*(−10)*				
	$\eta\eta$	−14.1	−14.1	0.27	−76.5	−76.5	–
		(−39)	*(−39)*				
{MnOsMn} **3**	$\xi\xi$	23.7	23.7	0.01	25.5	25.5	3
	$\zeta\zeta$	–	–	0.14	–	–	2
	η	11.1	11.1	–	22.5	22.5	–
	η	–	–	–	−102	−102	–

[a] The values shown in parentheses are spin-projected ones.

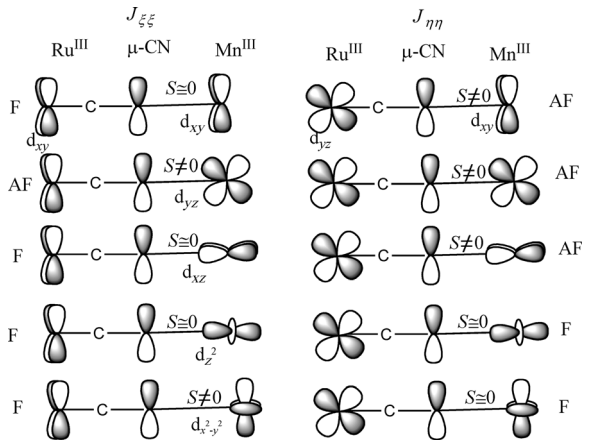

Figure 3. Representative orbital diagram qualitatively drawn from DFT-computed magnetic orbitals. The overlap integral (*S*) has been computed between the BS orbitals. See the Supporting Information for further details.

tion theory, which relates the projected exchange (denoted here as *J*′) to the orbital-dependent exchange by the following equation [Eq. (4)]:[30]

$$J_{1\zeta\zeta} = \left(-J'_{1\zeta\zeta} + J'_{1\xi\xi} + J'_{1\eta\eta}\right)/3$$
$$J_{1\xi\xi} = \left(-J'_{1\zeta\zeta} + J'_{1\xi\xi} - J'_{1\eta\eta}\right)/3 \quad (4)$$
$$J_{1\eta\eta} = \left(-J'_{1\zeta\zeta} + J'_{1\xi\xi} + J'_{1\eta\eta}\right)/3$$

Thus the final set of projected three-axis anisotropy can be obtained and these have been estimated for complexes **2** and **3**. For complex **2** the obtained values are $J'_{1\xi\xi}=7.5$ cm^{-1}, $J'_{1\zeta\zeta}=-9$ cm^{-1} and $J'_{1\eta\eta}=-76.5$ cm^{-1}, and our DFT calculations on projection yield $J'_{1\xi\xi}=7.5$ cm^{-1}, $J'_{1\zeta\zeta}=-10$ cm^{-1}, $J'_{1\eta\eta}=-39$ cm^{-1}. Here too the agreement is evident, even though the value of $J'_{1\eta\eta}$ is underestimated in our calculations. For complex **3**, the experimental projections yield values of $J'_{1\xi\xi}=25.5$ cm^{-1}, $J'_{1\zeta\zeta}=-22.5$ cm^{-1} and $J'_{1\eta\eta}=-102$ cm^{-1} for **3**; however, since we were unable to converge the $\eta\eta$ solution, we could not compute the projected *J*′ values for complex **3**.

To this end, we can see there is a reasonable agreement between the computed values (see Table 2), with the exception of the ($J_{1\eta\eta}/J'_{1\eta\eta}$) values for complex **2**. Although a deviation in the estimation of *J* values calculated by means of B3LYP relative to the experimental data has been witnessed in some cases in the literature,[35] the exact reason for underestimating this particular pair of exchanges is unclear and might be related to some structural distortions (see magneto–structural correlations).

To gain further insight into the nature of the computed magnetic coupling, an overlap integral analysis was performed and the results are summarised schematically in Figure 3.

The computed spin-density plots for HS configuration for all three electronic configurations of Ru^{III} discussed above are shown in Figure 4. The carbon atom of the bridging cyanide has small but a positive spin density when the unpaired electrons reside in the d_{xy} orbital and it is relatively large and negative when the unpaired electrons are located in the d_{xz}/d_{yz} orbitals. This indicates how magnetic exchange propagates and

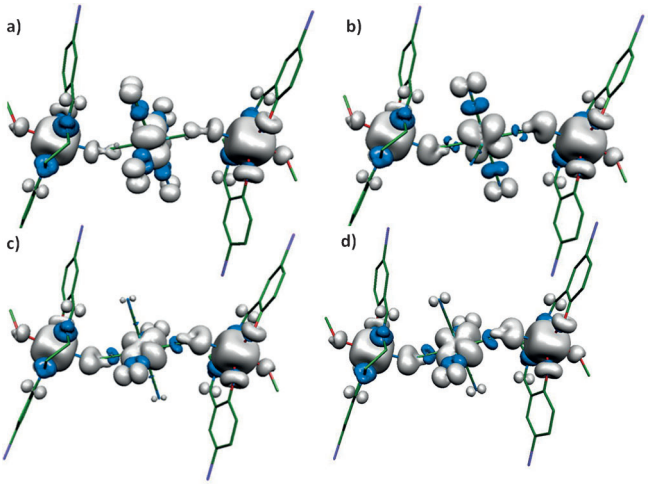

Figure 4. Spin-density plot for trinuclear complex **2** with $S=^9/_2$ and an isovalue of 0.002 e^{-1}bohr^{-3}: a) when the unpaired electron is in the d_{xy} orbital, b) when the unpaired electron is in the d_{yz} orbital, c) when the unpaired electron is in the d_{xz} orbital and d) when unpaired electron resides in the d_{xz} orbital of complex **3**.

how the orthogonality of the orbital plays a role in determining the sign and strength of the magnetic exchange. The nitrogen atoms of the bridging cyanides (coordinated to Mn^{III}) have large positive spin densities due to spin delocalisation from the Mn^{III}, whereas other atoms on the equatorial plane of the Mn^{III} ions have negative spin densities due to spin polarisation. This mixture of spin densities for Mn^{III} has been noted by us earlier.[51] As the J–T axis is along the cyanide bridge, the magnetic exchange interactions are relatively stronger.[11b] Across the series, Fe has a relatively large spin density (1.231) compared to Ru and Os (1.024 and 1.031).[52] The magnitude of spin densities indicates that all three ions gain spin density through a dominant spin-polarisation mechanism (see the spin-density plot for the all complexes **1**–**3** in Figure S3 of the Supporting Information; the magnetic orbitals and the spin densities are given in Figure S4 and Table S7, respectively, of the Supporting Information).

For complex **1** (see Table 3), the DFT calculations yield J_1 and J_2 values of $+3.5\ cm^{-1}$ relative to $+5.8\ cm^{-1}$ for the experimental values. A small but ferromagnetic J_3 interaction has been estimated for this complex. Consistent with other congeners, Fe^{III} also has the unpaired electron in the d_{xy} orbital and this essentially leads to ferromagnetic coupling with a similar mechanism proposed for the other analogues (see above). Only the $J_{\xi\xi}$ exchange has been considered here to help us understand the relative strength of the *J* values across the series in complexes **1**–**3**. As shown in Table 3, the *J* value decreases in the order 5d < 4d < 3d and this trend is also in agreement with the experimental results. The computed overlap integral values also reflect the observed trend (see Table S6 in the Supporting Information).

Zero-field splitting

Other than the spin ground-state value *S*, the ZFS is another important parameter for SMMs. In this series of complexes, the presence of two J–T elongated Mn^{III} ions with large single-ion ZFS can lead to relatively large cluster anisotropy. To estimate the Mn^{III} single-ion anisotropy and the cluster ($D_{9/2}$) anisotropy of complexes **1**–**3**, we have undertaken ab initio CASSCF as well as DFT calculations to estimate these parameters (see Table S8 in the Supporting Information). To estimate the single-ion ZFS, a monomeric Mn^{III} complex has been modelled from the trinuclear structure. Our DFT calculations yield a $D_{Mn^{III}}$ value of $-3.16\ cm^{-1}$, which is in excellent agreement with the $D_{Mn^{III}}$ of $-3.5\ cm^{-1}$ reported by experiments. Furthermore, a small *E*/*D* and an isotropic *g* tensor estimated for complex **3** by experimental results was also nicely reproduced in our B3LYP results. In many instances, it has been proposed that ab initio state-average CASSCF calculations that incorporate contributions from triplet states of Mn^{III} yield better estimates of the ZFS.[44] Thus we have also performed SA-CASSCF and NEVPT2 that incorporate dynamic correlation to estimate the single-ion ZFS. The computed values using these methodologies are summarised in Table 4. The estimate of *D* and *E*/*D* obtained from NEVPT2 is slightly superior to DFT estimates and this is in accord with the protocol proposed earlier.[44] The D_{SS} as well D_{SOC} individual contributions are also listed in Table 4. From these contributions, it is apparent that a large contribution to ZFS arises from the D_{SOC} parameter (85–90%).[44] The experimental *g* tensor is estimated to be $g_{Mn} \approx 1.98$, and our DFT values computed using the CPPP basis set are in agreement with these computed values. However, the NEVPT2 estimate of the *g* tensor is higher, and such an overestimation of the *g* tensor when using the CASSCF wave function has been previously detected in trinuclear Cu^{II} complexes.[53]

Table 4. DFT- and CASSCF/NEVPT2-calculated *D* tensor, D_{SS}, D_{SOC}, *E*/*D* and *g* tensor for the Mn monomer.

Method	D_{SS} [cm^{-1}]	D_{SOC} [cm^{-1}]	*D* [cm^{-1}]	*E*/*D*	$g_{Mn^{III}}$
B3LYP/CPPP	−1.17	−2.031	−3.20	0.06	1.99
BP86/TZVPPP	−0.01	−3.07	−3.08	0.03	2.62
NEVPT2	−0.01	−3.01	−3.28	0.06	2.62
experimental	–	–	−3.5	0.057	1.98

In addition to using DFT, we also computed the trinuclear ZFS ($D_{9/2}$), which is estimated to be $-1.09\ cm^{-1}$ for **3**. Although this parameter has not been directly estimated experimentally, the inelastic neutron scattering (INS) transition indicates that the anisotropy should be around $-1.68\ cm^{-1}$.[28] As is evident from the computed value, the ZFS drastically decreases as we go from $D_{Mn^{III}}$ to the cluster $D_{9/2}$ despite the fact that the J–T axes of two Mn^{III} are nearly co-linear. Various contributions to these ZFS estimates are listed in Table 5. When comparing the data, it is clear that the large difference between the two ZFS parameters arises due to the difference in α-SOMO→β-SOMO contributions; this is essentially due to the mixing of Os^{III} orbitals with the Mn^{III} and also because of the increase in the number of unpaired electrons, which elevate the energy required to flip, as proposed earlier for polynuclear $\{Mn_6^{III}\}$ cluster studies.[54] The orientation of ZFS for complex **3** is shown in Figure 5.

Table 5. Spin–flip excitations responsible for the spin–orbit interaction.[a]

Spin–flip excitations	Mn monomer	Complex **3**
SOMO–SOMO α→α	−0.424	−0.234
DOMO–DOMO β→β	−0.016	−0.055
SOMO–SOMO α→β	−1.544	−0.474
DOMO–VMO β→α	−0.010	0.012

[a] DOMO: doubly occupied molecular orbital; SOMO: singly occupied molecular orbital; VMO: virtual molecular orbital.

We have estimated the ZFS of the $D_{9/2}$ state for all three complexes in their ground-state $(d_{yz})^2(d_{xz})^2(d_{xy})^1$ configuration. This estimate helps to understand how the single-ion ZFS of $D_{Mn^{III}}$ translates into the ZFS of the cluster. The estimated $D_{9/2}$ ZFS for the Os^{III} analogue was found to be $-1.09\ cm^{-1}$, whereas for **2** it is $-1.12\ cm^{-1}$ and for complex **1** it is found to be $-0.92\ cm^{-1}$. All three values are drastically reduced relative to the value computed for the $D_{Mn^{III}}$ and, interestingly, the $D_{9/2}$ for all three complexes is similar. A large reduction in the $D_{9/2}$ values in these cases is due to a large reduction in the spin–flip α→β excitations (see Tables S9 and S10 in the Supporting Information) as mentioned earlier.[54] Despite the same *S* and a similar *D* values, the estimated barrier height differs for complexes **1**–**3**. Now the question is why.

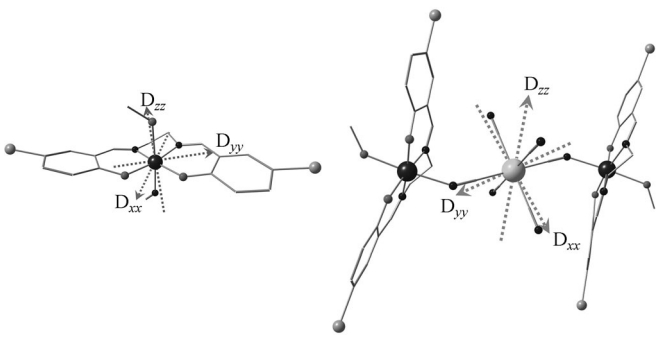

Figure 5. CASSCF-calculated orientation of ZFS for single-ion Mn^{III} (left) and the DFT-calculated orientation of the *D* tensor for complex **3**.

Orbital-dependent exchange and SMM behaviour

In this section, we focus our attention on understanding the role of orbital-dependent exchange in magnetisation-reversal barrier height in SMMs and how well the properties transform as we go down the periodic table from Fe to Os. The role of unquenched orbital angular momenta in enhancing the barrier height in SMMs is documented in a detailed theoretical work by Palli et al.[55] In particular, the magnetic anisotropy in the polynuclear complexes arises from the anisotropic response (*g* tensor) to the external magnetic field and the ZFS within the ground-state *S* manifold. Although the computed *g* tensors for three complexes are anisotropic, for simplicity we assume isotropic *g* tensors for all three complexes. If the magnetic exchange is isotropic in nature, the ZFS parameter essentially lifts the degeneracy of the *S* manifold; however, if the exchange is anisotropic in nature, the energy levels are drastically different. The spin spectra that focus only on the ground state and the first excited state with variety of scenarios are shown in Figure 6. The energy spectra of isotropic *J* values with and without ZFS are straightforward and do not require any explanation. For an anisotropic case with Ising-type $JS^z_{Os}S^z_{Mn}$ exchange (see Figure 6; all simulations were carried out using MAGPACK software.[56]), the reorientation barrier can be considerably larger compared to the isotropic counterpart.[18]

For the ferromagnetic ($J>0$) Ising-like spin coupling ($J_{\xi\xi}\neq 0$ and $J_{\eta\eta}=J_{\zeta\zeta}=0$), the spectrum is described by the $-JmM_S$ (here *m* and M_S denotes the *S* value of Os^{III} and Mn^{III}, respectively) pattern, which results in five doubly degenerate levels (see Figure S6 in the Supporting Information). The ground state is doubly degenerate with $M_z=\pm 5$ (see the Supporting Information for details). The ground state is separated from the excited state $M_z=\pm 3$ by $|J|/2$. It has been shown that in such a scenario the barrier height is determined approximately by the $|J|$ value or it can even be larger.[18] This suggests that the anisotropic exchange can lead to a larger barrier height than the isotropic exchange in polynuclear transition-metal complexes.

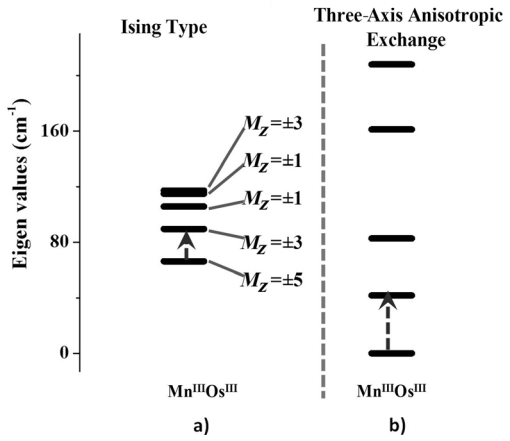

Figure 6. MAGPACK-computed spin-energy levels for the {MnOs} ferromagnetic exchange-coupled pair: a) Ising-type ferromagnetic interactions in {MnOs} ($J_{\xi\xi}=+25.5$ cm^{-1} and $J_{\zeta\zeta}=J_{\eta\eta}=0$). b) Anisotropic interaction in the {MnOs} ferromagnetically coupled pair ($J_{\xi\xi}=+25.5$ cm^{-1}, $J_{\eta\eta}=-102$ cm^{-1}, $J_{\zeta\zeta}=-22.5$ cm^{-1}). Single-ion ZFS of $D_{Mn^{III}}=-4.0$ cm^{-1} was considered during the MAGPACK simulations. The projection of the magnetisation along the *z* axis (M_z) is related to the *m* and M_S by $M_z=g_z(\mathrm{Os})m+g_z(\mathrm{Mn})M_S$, in which $g_z\approx 2.00$ for Os^{III} and $g_z\approx 2.00$ for the Mn^{III} for simplicity ($m={}^1/_2$ for Os^{III}, whereas $M_S=2$ for Mn^{III}).

Within the series studied, there are two sources of anisotropy, the first one being the single-ion anisotropy of Mn^{III} (ZFS; $D_{Mn^{III}}$), whereas the second contribution is due to the anisotropic exchange between the two pairs. As complexes **1**–**3** are nearly isostructural, the $D_{Mn^{III}}$ values are expected to be similar across the series. Thus the difference in the barrier height for reorientation of magnetisation must arise from the nature of anisotropic exchange exhibited by the individual pairs. Within our series studied, the Ru^{III} and the Os^{III} analogues exhibit three-axis anisotropic-type exchange (see *g* tensors computed for Kramers doublet in Table S3 of the Supporting Information).[28] However, the magnitude of the *J* values varies significantly between the two complexes. In particular, the $J_{\xi\xi}$ and $J_{\eta\eta}$ values differ significantly. This variation in the magnitude of *J* values along with the variation in sign led to difference in the ground-state/excited-state M_z gap. A comparison of Ising and three-axis exchange for the Mn^{III}–Os^{III} is shown in Figure 6 and this also illustrates the difference in the barrier that could arise due to the differing nature of the magnetic exchange. A stronger interaction observed in the case of Os eventually led to a larger ground-state/excited-state gap and thus a larger barrier height. A stronger interaction observed in the case of Os^{III} is routed back to a larger gap between different orbital-dependent configurations (see Figure 2). This is due to the larger and more diffused character of the 5d orbitals than 4d (Ru) and 3d (Fe) analogues. For Ru^{III}, on the other hand, a weaker overall anisotropic exchange[29] eventually reduces the gap between the ground-state/excited-state M_z gap and thus a reduction in the barrier height (see Figure S6 in the Supporting Information). Likewise for Fe analogues, a significant anisotropic exchange (that is, a non-zero $J_\perp$ value and likely to be antiferromagnetic as well) has been noted[28] and this again falls in the same category as that of the Ru^{III} analogue.

Moreover, as we go down in the series, the strength of the interaction significantly increases with $Os^{III}>Ru^{III}>Fe^{III}$ by 400 and 500% for Ru^{III} and Os^{III} analogues, respectively, relative to the *J* ($J_{\xi\xi}$) value of Fe^{III}. This enhanced *J* value leads to larger barrier heights for Os^{III} and Ru^{III} than the Fe^{III} analogue. We would like to note here that a similar Fe analogue has also been reported with barrier height as much as 30 K;[31] however, the crystal structure and magnetic properties of this complex are different to what we have studied here.[28] The difference in the magnetic properties, particularly the U_{eff}, is attributed to the difference in the α_{cis} angle (C-Fe-C *cis* angles) between these two structures. We have previously shown that this parameter is crucial in controlling the magnitude of anisotropy in cyanometalate complexes.[11b] In the next section, we will discuss the magneto–structural correlations developed for the Os^{III} analogue. These developed correlations offer clues about how to improve the effective barrier height by enhancing the strength of the magnetic exchange as discussed above.

Magneto–structural correlations

Magneto–structural correlations offer a way to further enhance the magnetic exchange by tuning a selected structural parameter. Within this series of complexes, we intend to develop correlations for complex **3**, as no correlations exist for the {Mn–Os} pair to date. The correlation has been done only on the ground state configuration, that is, only for the $J_{\xi\xi}$ interaction, whereas the other two directional anisotropies are likely to have different behaviour as they are involved in π-type interactions. Since Fe and Ru analogues are structurally similar, we believe a similar magneto–structural correlation to the one developed can be expected for these pairs. For cyano-bridged complexes, the most influential structural parameters are 1) the Os–C distance, 2) the Mn-N-C angle, 3) the Os-C-N bond angle and the Mn-N-C-Os dihedral angle.

Os–C distance

We started varying the Os–C distance related to $J_{1\xi\xi}$ (Os–Mn(1)) from 1.948 to 2.348 Å (Figure 8a). As the Os–C distance increases, the $J_{1\xi\xi}$ value decreases. The MOs and computed overlap integral reveals that as the Os–C distance increases, the carbon atoms develop a radical character (as evidenced from larger spin densities) and this eventually leads to larger Os(d_{xy})–Mn(d_{xz}) interaction, despite an increase in the distance between the metal ions. This large overlap eventually increases the antiferromagnetic contribution and leads to smaller $J_{1\xi\xi}$ values. Furthermore, as the metal–metal distance increases, there is also a sharp decrease in Os(d_{xy})–Mn($d_{x^2-y^2}$) cross-interaction, which leads to smaller *J* values. Since this interaction is essentially δ-type, the strength is correlated to distance. Quite interestingly, the $J_{2\xi\xi}$ interaction between Os–Mn(2) is significantly influenced by this parameter and in fact the $J_{2\xi\xi}$ interaction increases as the distance increases. What is evident from the computed spin densities is that increasing the Os–C distance alters the covalency of Os and its tendency for spin polarisation on the coordinated carbon atom decreases (see Table S11 in the Supporting Information) and this eventually leads to weaker overlap between magnetic orbitals at longer distance and stronger ferromagnetic exchange. This parameter particularly reveals that Os^{III} covalency is very subtle, and an asymmetric Os–C distance can lead to significantly different *J* values and might even lead to an $S = {}^1/_2$ ground state at some point. In addition, the $J_{3\xi\xi}$ interaction also changes; however, the magnitude of variation is rather small.

Mn-N-C bond angle

The experimental reports suggest that the Mn-N-C bond angle is the most sensitive structural parameter that governs the magnetic coupling and is often referred as the magic angle.[57] We have developed the magneto–structural correlations in which the angle is varied from 135 to 180°. As the bond angle increases, the ferromagnetic interaction between Mn and Os increases.[11c] At larger angles, the d_{xy} orbital of the Os^{III} is essentially orthogonal to the magnetic orbital of the Mn^{III} ions and this leads to an increase in ferromagnetic coupling. Furthermore, a significant cross interaction between the vacant Mn^{III} $d_{x^2-y^2}$ orbital with the Os–d_{xy} is also detected.[49] The spin-density analysis reveals that spin density on Os^{III} increases as we move towards the linear structure, which clearly reveals that the metal ion is strongly polarising at larger angles, and this leads to a larger $J_{\xi\xi}$ values (see Table S12 in the Supporting Information). The computed overlap integrals also support the developed magneto–structural correlations (see Table S13 in the Supporting Information).

OS-C-N angle

As we increase the angle around $J_{1\xi\xi}$, the magnitude of $J_{1\xi\xi}$ increases, whereas the $J_{2\xi\xi}$ interaction remains constant. The angle around the cyano carbon atom essentially leads to a linear Mn-C-N-Os arrangement at higher angles. As the structure tend towards linearity, the d_{xz} orbital of the Mn^{III} with which the d_{xy} of Os^{III} has a non-zero overlap will become strictly orthogonal (see Table S14 in the Supporting Information for the spin densities and Table S15 in the Supporting Information for overlap values). This leads to a decrease in the antiferromagnetic contribution and hence a large increase in the net $J_{1\xi\xi}$ values. The $J_{3\xi\xi}$ interaction also marginally decreases as we increase the angle. A consistent increase in the spin density of Os^{III} apparently leads to large $J_{\xi\xi}$ values.

ϕ parameter (cis to trans)

Due to the angle around nitrogen coordinated to Mn^{III}, the two Mn^{III} atoms are in *trans* position. By using the defined ϕ parameter (see Figure 8d, inset), we have developed a correlation in which we eventually go from the *trans* to the *cis* arrangement. The $J_{1\xi\xi}$ interaction shows a sinusoidal curve and a closer look at the MO reveals that as we rotate around the ϕ parameter the interaction of the d_{xz} orbital of Mn^{III} with the d_{xy} orbital of Os^{III} alters with a minimum overlap at 45 and 135°, thus leading to a maximum *J* value at this point (see Figure 7, which shows zero and non-zero overlap). The $J_{2\xi\xi}$ interaction is nearly constant, whereas $J_{3\xi\xi}$ significantly varies, and the interaction becomes weakly antiferromagnetic for the *cis* arrangement with a large ϕ parameter. A shorter Mn···Mn distance associated with larger ϕ parameter explains the larger variation observed (Figure 8).

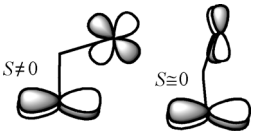

Figure 7. Schematic diagram for the interaction of the d_{xy} orbital of Os^{III} with the d_{xz} orbital of Mn^{III} by varying parameter φ.

Conclusion

In the past decade, there has been a great interest in the synthesis of and magnetic studies on Prussian blue analogues as they are attractive building blocks for SMMs. An alternate strategy has emerged in recent years in which mixed {3d–4d} and {3d–5d} clusters have been synthesised, and these were proven to be superior to 3d-only clusters in many instances.

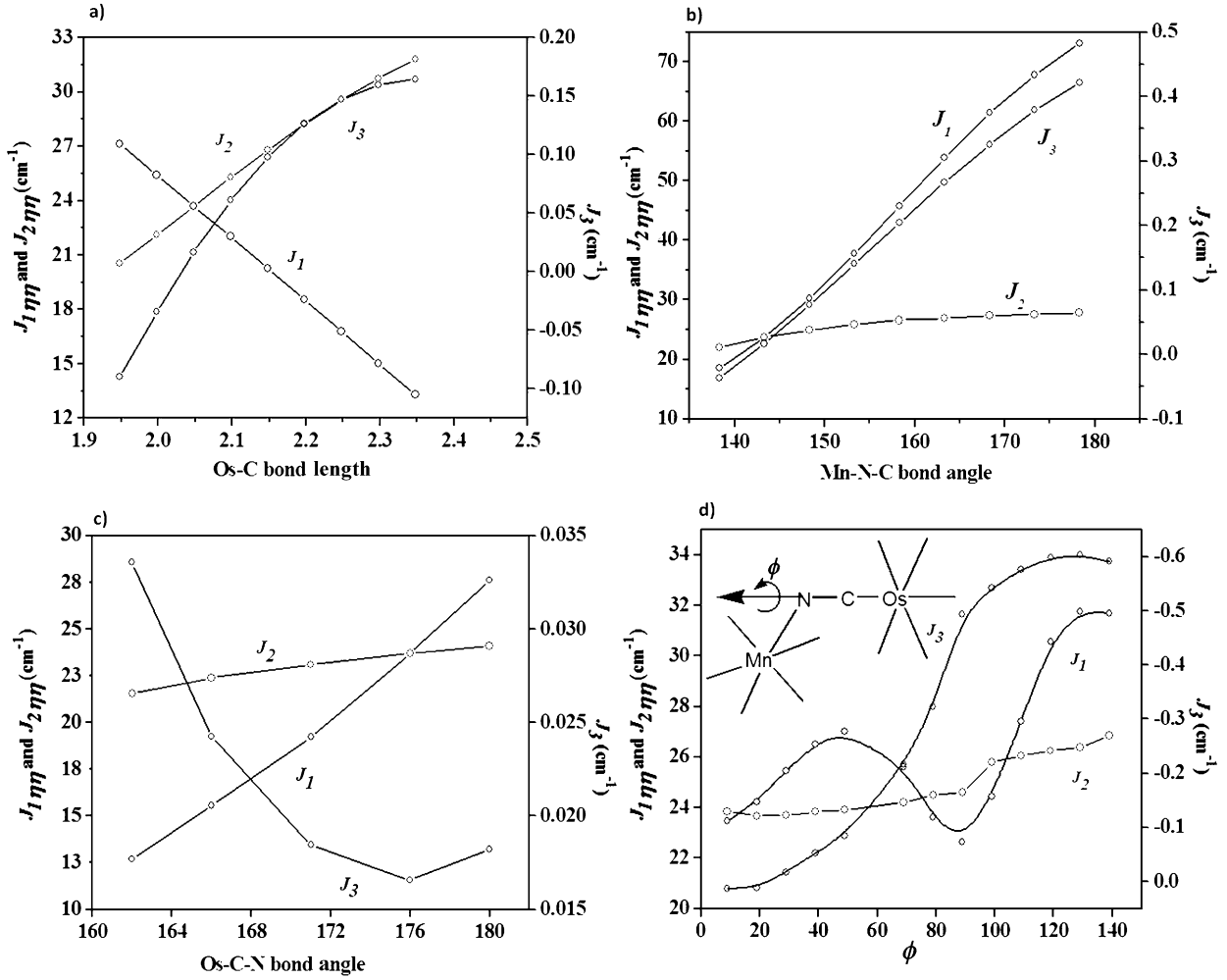

Figure 8. DFT-developed magneto–structural correlations for complex **3** by varying different structural parameters: a) Os–C distance, b) Mn-N-C bond angle, c) Os-C-N bond angle, d) parameter φ.

Although theoretical methods that demonstrate the role of 4d/5d metals in enhancing the barrier height reversal had been pursued earlier, a comprehensive DFT study coupled with CASSCF calculations that illustrates the advantages of this class of compounds has been lacking. For the first time, we have tackled this issue by thorough density functional calculations on a set of trinuclear {Mn^{III}-M^{III}-Mn^{III}} (in which M = Fe, Ru, Os) cyanometalate SMMs. The conclusions derived from this work can be summarised as follows:

1) The combination of B3LYP along with the effective-core potential basis set when analysing $Fe^{III}/Ru^{III}/Os^{III}$ yields an excellent estimate of the exchange coupling constants for complexes **1**–**3** relative to experimental results. As we go down in the series, a trend of $Os^{III} > Ru^{III} > Fe^{III}$ has been observed for the magnetic exchange interaction $J_{\xi\xi}$. Compared to the $J_{\xi\xi}$ value of Fe, the strength of the interaction increases by 400 and 500% for Ru and Os analogues, respectively.
2) The DFT calculations suggest that the ground state for the central d^5 low-spin cyanometalate system is $(d_{xz})^2(d_{yz})^2(d_{xy})^1$, with the unpaired electron being in the δ-type d_{xy} orbital. The CASSCF computation also echoes a similar pattern, with other two possible degenerate states lying closer to the ground state for Fe and Ru and far away for Os.
3) For the first time the orbital-dependent exchange has been successfully computed for a trinuclear complex by using DFT for the Os^{III} and Ru^{III} analogues. The computed *J* values (both non-projected and projected for Ru^{III} and non-projected for Os^{III}) are in agreement with the recent thorough experimental studies, although the exchange interaction due to the d_{yz} orbital is underestimated in our calculations. Our calculations clearly reiterate the observation of three-axis anisotropy for these two complexes and suggest that this protocol can be employed to perform a preliminary check on complexes that possess such anisotropic interactions.
4) Our MO and overlap integral analysis reveals that, apart from near-orthogonality of the $Os(d_{xy})$ orbital with other magnetic orbitals of Mn^{III}, a cross-interaction between the $Os(d_{xy})$ and the vacant $Mn(d_{x^2-y^2})$ orbital lead to an overall ferromagnetic Ising-type exchange for this pair. Interestingly, this interaction was found to decrease significantly as we go from Os to Fe in the series, and this leads to smaller *J*

values for the Ru and Fe analogues. The larger and more diffused nature of the 4d and 5d orbitals than the 3d orbitals of Fe is also evident from the computed spin densities on the metal as well as the bridging cyanide moiety.

5) CASSCF and DFT calculations have been employed to estimate the single-ion ZFS of Mn^{III}, and the computed values are in excellent agreement with the experimentally reported values. The ZFS values calculated for the $S=^9/_2$ state using DFT for all three complexes are nearly same and this suggests that the ZFS of the Mn^{III} or the ground state is unlikely to affect the barrier height reversal for complexes **1**–**3**.
6) Our calculations reveal that the nature of exchange coupling (isotropic, Ising and anisotropic exchange) is likely the factor that leads to a difference in the barrier height for the reversal of magnetisation in complexes **1**–**3**.
7) The developed magneto–structural correlations suggest that the Mn-N-C bond angle is an important parameter and a larger angle enhances the strength of the exchange. Since the strength of the exchange interaction is related to the barrier height reversal here, a large Mn-N-C bond angle is likely to yield a superior SMM.

Acknowledgements

G.R. would like to acknowledge financial support from the Government of India through the Department of Science and Technology (SR/S1/IC-41/2010, SR/NM/NS-1119/2011) and the Indian Institute of Technology, Bombay for access to the high performance computing facility. S.K.S. would like to thank CSIR New Delhi for an SRF fellowship.

Keywords: cyanometalates · density functional calculations · magnetic properties · osmium · ruthenium

[1] a) R. Sessoli, D. Gatteschi, A. Caneschi, M. A. Novak, *Nature* **1993**, *365*, 141; b) G. Christou, D. Gatteschi, D. N. Hendrickson, R. Sessoli, *Mater. Res. Bull.* **2000**, *35*, 66; c) D. Gatteschi, R. Sessoli, J. Villain, *Molecular Nanomagnets*, Oxford University Press, Oxford, **2006**.

[2] a) M. Leuenberger, D. Loss, *Nature* **2001**, *410*, 789; b) S. Hill, R. S. Edwards, N. Alliaga-Alcalde, G. Christou, *Science* **2003**, *302*, 1015; c) M. Affronte, F. Troiani, A. Ghirri, A. Candini, M. Evangelisti, V. Corradini, S. Carretta, P. Santini, G. Amoretti, F. Tuna, G. Timco, R. E. P. Winpenny, *J. Phys. D* **2007**, *40*, 2999; d) R. E. P. Winpenny, *Angew. Chem.* **2008**, *120*, 8112; *Angew. Chem. Int. Ed.* **2008**, *47*, 7992; e) A. Ardavan, O. Rival, J. J. L. Morton, S. J. Blundell, A. M. Tyryshkin, G. A. Timco, R. E. P. Winpenny, *Phys. Rev. Lett.* **2007**, *98*, 057201; f) G. Aromi, D. Aguila, P. Gamez, F. Luisc, O. Roubeauc, *Chem. Soc. Rev.* **2012**, *41*, 537.

[3] a) F. K. Larsen, E. J. L. McInnes, H. El. Mkami, J. Overgaard, S. Piligkos, G. Rajaraman, E. Rentschler, A. A. Smith, G. M. Smith, V. Boote, M. Jennings, G. A. Timco, R. E. P. Winpenny, *Angew. Chem.* **2003**, *115*, 105; *Angew. Chem. Int. Ed.* **2003**, *42*, 101; b) M. Affronte, F. Troiani, A. Ghirri, S. Carretta, P. Santini, V. Corradini, R. Schuecker, C. Muryn, G. Timco, R. E. P. Winpenny, *Dalton Trans.* **2006**, 2810; c) F. Troiani, A. Ghirri, M. Affronte, S. Carretta, P. Santini, G. Amoretti, S. Piligkos, G. Timco, R. E. P. Winpenny, *Phys. Rev. Lett.* **2005**, *94*, 207208; d) J. M. Clemente-Juan, E. Coronado, A. Gaita-Arino, *Coord. Chem. Rev.* **2012**, *41*, 7464.

[4] a) C. J. Milios, A. Vinslava, W. Wernsdorfer, S. Moggach, S. Parsons, S. P. Perlepes, G. Christou, E. K. Brechin, *J. Am. Chem. Soc.* **2007**, *129*, 2754; b) *Molecular Cluster Magnets, Vol. 3* (Ed.: R. E. P. Winpenny) World Scientific Series in Nanoscience and Nanotechnology, Singapore, **2011**; c) *Single-Molecule Magnets and Related Phenomena* (Ed.: R. E. P. Winpenny), Springer, Berlin, **2006**.

[5] a) C. J. Milios, A. Vinslava, W. Wernsdorfer, A. Prescimone, P. A. Wood, S. Parsons, S. P. Perlepes, G. Christou, E. K. Brechin, *J. Am. Chem. Soc.* **2007**, *129*, 6547; b) C. J. Milios, R. Inglis, A. Vinslava, R. Bagai, W. Wernsdorfer, S. Parsons, S. P. Perlepes, G. Christou, E. K. Brechin, *J. Am. Chem. Soc.* **2007**, *129*, 12505.

[6] R. E. P. Winpenny, *J. Chem. Soc. Dalton Trans.* **2002**, 1.

[7] R. Sessoli, H.-L. Tsai, A. R. Schake, S. Wang, J. B. Vincent, K. Folting, D. Gatteschi, G. Christou, D. N. Hendrickson, *J. Am. Chem. Soc.* **1993**, *115*, 1804.

[8] A. J. Tasiopoulos, A. Vinslava, W. Wernsdorfer, K. A. Abboud, G. Christou, *Angew. Chem.* **2004**, *116*, 2169; *Angew. Chem. Int. Ed.* **2004**, *43*, 2117.

[9] L. M. C. Beltran, J. R. Long, *Acc. Chem. Res.* **2005**, *38*, 325.

[10] a) G. Aromí, P. Gamez, J. Krzystek, H. Kooijman, A. L. Spek, E. J. MacLean, S. J. Teat, H. Nowell, *Inorg. Chem.* **2007**, *46*, 2519; b) G. Aromí, H. Stoeckli-Evans, S. J. Teat, J. Cano, J. Ribas, *J. Mater. Chem.* **2006**, *16*, 2635; c) G. Aromí, P. Gamez, J. Reedijk, *Coord. Chem. Rev.* **2008**, *252*, 964; d) G. Aromí, P. Gamez, O. Roubeau, P. C. Berzal, H. Kooijman, H. A. L. Spek, W. L. Driessen, J. Reedijk, *Inorg. Chem.* **2002**, *41*, 3673; e) V. A. Grillo, E. J. Seddon, C. M. Grant, G. Aromí, J. C. Bollinger, K. Folting, G. Christou, *Chem. Commun.* **1997**, 1561.

[11] a) M. Atanasov, P. Comba, S. Hausberg, B. Martin, *Coord. Chem. Rev.* **2009**, *253*, 2306; b) M. Atanasov, C. Busche, P. Comba, F. El Hallak, B. Martin, G. Rajaraman, J. van Slageren, H. Wadepohl, *Inorg. Chem.* **2008**, *47*, 8112; c) M. Atanasov, P. Comba, C. A. Daul, *J. Phys. Chem. A* **2006**, *110*, 13332; d) M. Atanasov, P. Comba, S. Förster, G. Linti, T. Malcherek, R. Miletich, A. I. Prikhod'ko, H. Wadepohl, *Inorg. Chem.* **2006**, *45*, 7722; e) M. Atanasov, P. Comba, C. A. Daul, *Inorg. Chem.* **2008**, *47*, 2449; f) M. Atanasov, P. Comba, S. Helmle, *Inorg. Chem.* **2012**, *51*, 9357; g) M. Atanasov, P. Comba, S. Helmle, D. Muller, F. Neese, *Inorg. Chem.* **2012**, *51*, 12324.

[12] a) S. Ferlay, T. Mallah, R. Ouahès, P. Veillet, M. Verdaguer, *Nature* **1995**, *378*, 701; b) M. Verdaguer, A. Bleuzen, V. Marvaud, J. Vaissermann, M. Seuleiman, C. Desplanches, A. Scuiller, C. Train, R. Garde, G. Gelly, C. Lomenech, I. Rosenman, P. Veillet, C. Cartier, F. Villain, *Coord. Chem. Rev.* **1999**, *192*, 1023; c) S. Ferlay, T. Mallah, R. Ouahes, P. Veillet, M. Verdaguer, *Inorg. Chem.* **1999**, *38*, 229; d) M. Verdaguer, F. Villain, R. Ouahès, N. Galvez, R. Garde, G. Keller, F. Tournilhac, *Polyhedron* **2005**, *24*, 2906; e) T. Glaser, I. Liratzis, A. M. Ako, A. K. Powell, *Coord. Chem. Rev.* **2009**, *253*, 2296; f) T. Glaser, *Coord. Chem. Rev.* **2013**, *257*, 140.

[13] a) E. Ruiz, G. Rajaraman, S. Alvarez, B. Gillon, J. Stride, R. Clèrac, J. Larionova, S. Decurtins, *Angew. Chem.* **2005**, *117*, 2771; *Angew. Chem. Int. Ed.* **2005**, *44*, 2711; b) D. Visinescu, C. Desplanches, I. Imaz, V. Bahers, R. Pradhan, F. A. Villamena, P. Guionneau, J.-P. Sutter, *J. Am. Chem. Soc.* **2006**, *128*, 10202.

[14] A. G. Sharpe, *The Chemistry of Cyano Complexes of the Transition Metals*, Academic Press, New York, **1976**.

[15] a) K. R. Dunbar, R. A. Heintz, *Prog. Inorg. Chem.* **1996**, *45*, 283; b) J. S. Miller, J. L. Manson, *Acc. Chem. Res.* **2001**, *34*, 563; c) M. Shatruk, C. Avendano, K. R. Dunbar, *Prog. Inorg. Chem.* **2009**, *56*, 155.

[16] a) B. Sieklucka, R. Podgajny, P. Przychodzen, T. Korzeniak, *Coord. Chem. Rev.* **2005**, *249*, 2203; b) J. Martinez-Lillo, D. Armentano, G. De Munno, G. W. Wernsdorfer, M. Julve, F. Lloret, J. Faus, *J. Am. Chem. Soc.* **2009**, *131*, 14218; c) J. J. Sokol, A. G. Hee, J. R. Long, *J. Am. Chem. Soc.* **2002**, *124*, 7656; d) F. Karadas, C. Avendano, M. G. Hilfiger, A. V. Prosvirin, K. R. Dunbar, *Dalton Trans.* **2010**, *39*, 4968; e) Y. Song, P. X. Zhang, M. Ren, X. F. Shen, Y. Z. Li, X. Z. You, *J. Am. Chem. Soc.* **2005**, *127*, 3708.

[17] X. Y. Wang, C. Avendanoa, K. R. Dunbar, *Chem. Soc. Rev.* **2011**, *40*, 3213.

[18] a) V. S. Mironov, L. F. Chibotaru, A. Ceulemans, *J. Am. Chem. Soc.* **2003**, *125*, 9750; b) V. S. Mironov, *Dokl. Phys. Chem.* **2007**, *415*, 199; c) V. S. Mironov, *Dokl. Phys. Chem.* **2004**, *397*, 154.

[19] A. Bleuzen, V. Marvaud, C. Mathoniere, B. Sieklucka, M. Verdaguer, *Inorg. Chem.* **2009**, *48*, 3453 and references therein.

[20] a) M. Arai, W. Kosaka, T. Matsuda, S. Ohkoshi, *Angew. Chem.* **2008**, *120*, 6991; *Angew. Chem. Int. Ed.* **2008**, *47*, 6885; b) O. Sato, T. Iyoda, A. Fujishima, K. Hashimoto, *Science* **1996**, *272*, 704; c) C. Mathonière, R. Podgajny, P. Guionneau, C. Labrugere, B. Sieklucka, *Chem. Mater.* **2005**, *17*, 442.

[21] a) M. Ferbinteanu, H. Miyasaka, W. Wernsdorfer, K. Nakata, K. Sugiura, M. Yamashita, C. Coulon, R. Clerac, *J. Am. Chem. Soc.* **2005**, *127*, 3090; b) H. Miyasaka, M. Julve, M. Yamashita, R. Cle'rac, *Inorg. Chem.* **2009**, *48*, 3420; c) N. E. Chakov, W. Wernsdorfer, K. A. Abboud, G. Christou, *Inorg. Chem.* **2004**, *43*, 5919.

[22] G. S. Girolami, W. R. Entley, *Science* **1995**, *268*, 397.

[23] a) V. Chandrasekhar, J. Goura, E. C. Saunado, *Inorg. Chem.* **2012**, *51*, 8479; b) V. Chandrasekhar, T. Senapati, A. Dey, S. Hossain, *Dalton Trans.* **2011**, *40*, 5394; c) V. Chandrasekhar, T. Senapati, A. Dey, E. C. Saunado, *Inorg. Chem.* **2011**, *50*, 1420; d) V. Chandrasekhar, T. Senapati, E. C. Saunado, R. Clèrac, *Inorg. Chem.* **2009**, *48*, 6192.

[24] a) S. Khanra, M. Kloth, H. Mansaray, C. A. Muryn, F. Tuna, E. C. Sanudo, M. Helliwell, E. J. L. McInnes, R. E. P. Winpenny, *Angew. Chem.* **2007**, *119*, 5664; *Angew. Chem. Int. Ed.* **2007**, *46*, 5568; b) E. K. Brechin, R. A. Coxall, A. Parkin, S. Parsons, P. A. Tasker, R. E. P. Winpenny, *Angew. Chem.* **2001**, *113*, 2772; *Angew. Chem. Int. Ed.* **2001**, *40*, 2700; c) Y.-Z. Zheng, M. Evangelisti, R. E. P. Winpenny, *Angew. Chem.* **2011**, *123*, 3776; *Angew. Chem. Int. Ed.* **2011**, *50*, 3692; d) S. Maheswaran, G. Chastanet, S. J. Teat, T. Mallah, R. Sessoli, W. Wernsdorfer, R. E. P. Winpenny, *Angew. Chem.* **2005**, *117*, 5172; *Angew. Chem. Int. Ed.* **2005**, *44*, 5044.

[25] a) A. Palii, S. M. Ostrovsky, S. I. Klokishner, B. S. Tsukerblat, K. R. Dunbar, *ChemPhysChem* **2006**, *7*, 871; b) A. V. Palii, S. M. Ostrovsky, S. I. Klokishner, B. S. Tsukerblat, C. P. Berlinguette, K. R. Dunbar, J. R. Galan-Mascaros, *J. Am. Chem. Soc.* **2004**, *126*, 16860; c) A. V. Palii, B. S. Tsukerblat, M. Verdaguer, *J. Chem. Phys.* **2002**, *117*, 7896.

[26] E. Ruiz, A. Rodríguez-Fortea, S. Alvarez, M. Verdaguer, *Chem. Eur. J.* **2005**, *11*, 2135.

[27] L. F. Chibotaru, V. S. Mirnov, A. Ceulemans, *Angew. Chem.* **2001**, *113*, 4561; *Angew. Chem. Int. Ed.* **2001**, *40*, 4429.

[28] K. S. Pedersen, M. Schau-Magnussen, J. Bendix, H. Weihe, H. A. V. Palli, S. I. Klokishner, S. Ostrovsky, O. S. Reu, H. Mutka, P. L. W. Tregenna-Piggott, *Chem. Eur. J.* **2010**, *16*, 13458.

[29] K. S. Pedersen, J. Dreiser, J. Nehrkorn, M. Gysler, M. Schau-Magnussen, A. Schnegg, K. Holldack, R. Bittl, S. Piligkos, H. Weihe, P. L. W. Tregenna-Piggott, O. Waldmann, J. Bendix, *Chem. Commun.* **2011**, *47*, 6918.

[30] J. Dreiser, K. S. Pedersen, A. Schnegg, K. Holldack, J. Nehrkorn, M. Sigrist, P. Tregenna-Piggott, H. Mukta, H. Weihe, V. S. Mironov, J. Bendix, O. Waldmann, *Chem. Eur. J.* **2013**, *19*, 3693.

[31] H. J. Choi, J. J. Sokol, J. R. Long, *Inorg. Chem.* **2004**, *43*, 1606.

[32] See ref. [21a].

[33] J. Dreiser, A. Schnegg, K. Holldack, K. S. Pedersen, M. Schau-Magnussen, J. Nehrkorn, P. Tregenna-Piggott, H. Mukta, H. Weihe, J. Bendix, O. Waldmann, *Chem. Eur. J.* **2011**, *17*, 7492.

[34] P. L. W. Tregenna-Piggott, D. Sheptyakov, L. Keller, S. I. Klokishner, S. Ostrovsky, A. V. Palli, O. S. Reu, J. Bendix, T. Brock-Nannestad, K. S. Pedersen, H. Weihe, H. Mutka, *Inorg. Chem.* **2010**, *49*, 13458.

[35] E. Ruiz, S. Alvarez, A. Rodriguez-Fortea, P. Alemany, Y. Pouillon, C. Massobrio in *Magnetism: Molecules to Materials, Vol. II* (Eds.: J. S. Miller, M. Drillon), Wiley-VCH, Weinheim, **2001**, p. 227; a) S. Piligkos, G. Rajaraman, M. Soler, N. Kirchner, J. van Slageren, R. Bircher, S. Parsons, H. Guedel, J. Kortus, W. Wernsdorfer, G. Christou, E. K. Brechin, *J. Am. Chem. Soc.* **2005**, *127*, 5572; b) E. Ruiz, S. Alvarez, J. Cano, P. Alemany, *J. Comput. Chem.* **1999**, *20*, 1391; c) E. Ruiz, A. R. Fortea, J. Cano, S. Alvarez, P. Alemany, *J. Comput. Chem.* **2003**, *24*, 982; d) E. Ruiz, J. Cano, S. Alvarez, A. Caneschi, D. Gatteschi, *J. Am. Chem. Soc.* **2003**, *125*, 6791; e) G. Rajaraman, J. Cano, E. K. Brechin, E. J. L. McInnes, *Chem. Commun.* **2004**, 1476; f) M. Shoji, Y. Kitagawa, T. Kawakami, S. Yamanaka, M. Okumura, K. Yamaguchi, *J. Phys. Chem. A* **2008**, *112*, 4020; g) T. Ishida, T. Kawakami, S.-I. Mitsubori, T. Nogamo, K. Yamaguchi, H. Iwamura, *Dalton Trans.* **2002**, 3177; h) M. Nishino, Y. Yoshioka, K. Yamaguchi, *Chem. Phys. Lett.* **1998**, *297*, 51; i) S. K. Singh, G. Rajaraman, *Dalton Trans.* **2013**, *42*, 3623; j) S. K. Singh, N. K. Tibrewal, G. Rajaraman, *Dalton Trans.* **2011**, *40*, 10897; k) T. Rajeshkumar, S. K. Singh, G. Rajaraman, *Polyhedron* **2013**, *52*, 1299; l) T. Rajeshkumar, G. Rajaraman, *Chem. Commun.* **2012**, *48*, 7856; m) S. K. Singh, K. S. Pederson, M. Sirgist, C. Aa. Thuesen, M. Schau-Magnussen, H. Mutka, S. Piligkos, H. Weighe, G. Rajaraman, J. Bendix, *Chem. Commun.* **2013**, *49*, 5583.

[36] Gaussian 09, Revision A.01, M. J. Frisch, G. W. Trucks, H. B. Schlegel, G. E. Scuseria, M. A. Robb, J. R. Cheeseman, G. Scalmani, V. Barone, B. Mennucci, G. A. Petersson, H. Nakatsuji, M. Caricato, X. Li, H. P. Hratchian, A. F. Izmaylov, J. Bloino, G. Zheng, J. L. Sonnenberg, M. Hada, M. Ehara, K. Toyota, R. Fukuda, J. Hasegawa, M. Ishida, T. Nakajima, Y. Honda, O. Kitao, H. Nakai, T. Vreven, J. A. Montgomery, Jr., J. E. Peralta, F. Ogliaro, M. Bearpark, J. J. Heyd, E. Brothers, K. N. Kudin, V. N. Staroverov, R. Kobayashi, J. Normand, K. Raghavachari, A. Rendell, J. C. Burant, S. S. Iyengar, J. Tomasi, M. Cossi, N. Rega, J. M. Millam, M. Klene, J. E. Knox, J. B. Cross, V. Bakken, C. Adamo, J. Jaramillo, R. Gomperts, R. E. Stratmann, O. Yazyev, A. J. Austin, R. Cammi, C. Pomelli, J. W. Ochterski, R. L. Martin, K. Morokuma, V. G. Zakrzewski, G. A. Voth, P. Salvador, J. J. Dannenberg, S. Dapprich, A. D. Daniels, Ö. Farkas, J. B. Foresman, J. V. Ortiz, J. Cioslowski, D. J. Fox, Gaussian, Inc., Wallingford CT, **2009**.

[37] A. D. Becke, *J. Chem. Phys.* **1993**, *98*, 5648.

[38] a) P. J. Hay, W. R. Wadt, *J. Chem. Phys.* **1985**, *82*, 299; b) L. E. Roy, P. J. Hay, R. L. Martin, *J. Chem. Theory Comput.* **2008**, *4*, 1029; c) A. W. Ehlers, M. Bohme, S. Dapprich, A. Gobbi, A. Hollwarth, V. Jonas, K. F. Kohler, R. Stegmann, A. Veldkamp, G. Frenking, *Chem. Phys. Lett.* **1993**, *208*, 111.

[39] a) P. J. Hay, W. R. Wadt, *J. Chem. Phys.* **1985**, *82*, 270; b) P. J. Hay, W. R. Wadt, *J. Chem. Phys.* **1985**, *82*, 284; c) see ref. [38a].

[40] A. Schäfer, C. Huber, R. Ahlrichs, *J. Chem. Phys.* **1994**, *100*, 5829.

[41] F. Neese, Orca 2.9, Mullheim an der Ruhr, Germany, **2011**.

[42] D. Ganyushin, F. Neese, *J. Chem. Phys.* **2006**, *125*, 024103.

[43] D. A. Pantazis, X.-Y. Chen, C. R. Landis, F. Neese, *J. Chem. Theory Comput.* **2008**, *4*, 908.

[44] a) C. Duboc, D. Ganyushin, K. Sivalingam, M.-N. Collomb, F. Neese, *J. Phys. Chem. A* **2010**, *114*, 10750; b) F. Neese, T. Petrenko, D. Ganyushin, G. Olbrich, *Coord. Chem. Rev.* **2007**, *251*, 288; c) F. Neese, *J. Am. Chem. Soc.* **2006**, *128*, 10213; d) D. Maganas, S. Sottini, P. Kyritsis, E. J. J. Groenen, F. Neese, *Inorg. Chem.* **2011**, *50*, 8741.

[45] M. Douglas, N. M. Kroll, *Ann. Phys.* **1974**, *82*, 89.

[46] a) C. Angeli, R. Cimiraglia, S. Evangelisti, T. Leininger, J. P. Malrieu, *J. Chem. Phys.* **2001**, *114*, 10252; b) C. Angeli, R. Cimiraglia, T. Leininger, J. P. Malrieu, *Chem. Phys. Lett.* **2001**, *350*, 297; c) C. Angeli, R. Cimiraglia, T. Leininger, J. P. Malrieu, *J. Chem. Phys.* **2002**, *117*, 9138.

[47] F. Aquilante, L. De Vico, N. Ferré, G. Ghigo, P. Malmqvist, P. Neogrády, T. B. Pedersen, M. Pitoňák, M. Reiher, B. O. Roos, L. Serrano-Andrés, M. Urban, V. Veryazov, R. Lindh, *J. Comput. Chem.* **2010**, *31*, 224.

[48] K. Meyer, E. Bill, B. Mienert, T. Weyhermuller, K. Wieghardt, *J. Am. Chem. Soc.* **1999**, *121*, 4859.

[49] a) L. F. Chibotaru, L. Ungur, *Phys. Rev. Lett.* **2012**, *109*, 246403; b) L. F. Chibotaru, A. Ceulemans, H. Bolvin, *Phys. Rev. Lett.* **2008**, *101*, 033003; c) L. Ungur, L. F. Chibotaru, *J. Chem. Phys.* **2012**, *137*, 064112.

[50] A. Ceulemans, G. A. Heylen, L. F. Chibotaru, T. L. Maes, K. Pierloot, C. Ribbing, L. G. Vanquickenborne, *Inorg. Chim. Acta* **1996**, *251*, 15.

[51] a) N. Berg, T. Rajeshkumar, S. M. Taylor, E. K. Brechin, G. Rajaraman, L. F. Jones, *Chem. Eur. J.* **2012**, *18*, 5906; b) L. F. Jones, G. Rajaraman, J. Brockman, M. Murugesu, E. C. Sanudo, J. Raftery, S. J. Teat, W. Wernsdorfer, G. Christou, E. K. Brechin, D. Collison, *Chem. Eur. J.* **2004**, *10*, 5180.

[52] a) J. Bendix, P. Steenberg, I. Søtofte, *Inorg. Chem.* **2003**, *42*, 4510; b) P. Albores, L. D. Slep, L. M. Baraldo, R. Baggio, M. T. Garland, E. Rentschler, *Inorg. Chem.* **2006**, *45*, 2361.

[53] S. Vancoillie, J. Chalupsky, U. Ryde, E. I. Solomon, K. Pierloot, F. Neese, L. Rulısek, *J. Phys. Chem. B* **2010**, *114*, 7692.

[54] E. Ruiz, J. Cirera, J. Cano, S. Alvarez, C. Loose, J. Kortus, *Chem. Commun.* **2008**, *1*, 52.

[55] a) A. Palii, B. S. Tsukerblat, J. M. Clemente-Juan, E. Coronado, *Int. Rev. Phys. Chem.* **2010**, *29*, 135; b) A. Palii, B. S. Tsukerblat, S. Klokishner, K. R. Dunbar, J. M. Clemente-Juan, E. Coronado, *Chem. Soc. Rev.* **2011**, *40*, 3130.

[56] J. J. Borras-Almenar, J. M. Clemente-Juan, E. Coronado, B. S. Tsukerblat, *J. Comput. Chem.* **2001**, *22*, 985.

[57] a) J. M. Herrera, A. Bachschmidt, F. Villain, A. Bleuzen, V. Marvaud, W. Wernsdorfer, M. Verdaguer, *Phil. Trans. R. Soc. A* **2008**, *366*, 127; b) H. Miyasaka, N. Matsumoto, N. Re, E. Gallo, C. Floriani, *Inorg. Chem.* **1997**, *36*, 670.

Received: September 4, 2013
Published online on November 29, 2013